Scanning Electron Microscopy

Volume 1982
Number 1 *1982*

Article 23

1982

Analytical Scanning Electron Microscopy for Surface Science

Olive Lee-Deacon
CEN-Saclay

Claude Le Gressus
CEN-Saclay

Daniel Massignon
CEN-Saclay

Follow this and additional works at: https://digitalcommons.usu.edu/electron

Part of the Biology Commons

Recommended Citation

Lee-Deacon, Olive; Le Gressus, Claude; and Massignon, Daniel (1982) "Analytical Scanning Electron Microscopy for Surface Science," *Scanning Electron Microscopy*: Vol. 1982 : No. 1 , Article 23.
Available at: https://digitalcommons.usu.edu/electron/vol1982/iss1/23

This Article is brought to you for free and open access by the Western Dairy Center at DigitalCommons@USU. It has been accepted for inclusion in Scanning Electron Microscopy by an authorized administrator of DigitalCommons@USU. For more information, please contact digitalcommons@usu.edu.

Electron Beam Interactions With Solids (Pp. 271-279)
SEM, Inc., AMF O'Hare (Chicago), IL 60666, U.S.A.

ANALYTICAL SCANNING ELECTRON MICROSCOPY FOR SURFACE SCIENCE

Olive Lee-Deacon, Claude Le Gressus,* Daniel Massignon

DESICP, CEN-Saclay, 91191 Gif-sur-Yvette, France

*Responsible for correspondence, Tel: 908-47-62

ABSTRACT

To correlate an electron image with surface properties requires thorough understanding of electron-solid interaction, secondary electron emission mechanism and operation functions of image detectors. We emphasize the importance and usefulness of combining electron spectroscopy with scanning electron microscope in interpreting electron image contrast. Linear relationships among secondary electron image (SEI) brightness, total emission current and the integration of electron energy distribution were measured. We propose that channeling effect, instead of primary electron diffraction, is the crystallographic cause of SEI contrast. Secondary electrons contribute most to SEI brightness because of their high constituent in total yield, not because of high efficiency of SEI detector in detecting slow electrons. We show that work function change alone cannot explain the SEI brightness change during gas exposure. Rather, the brightness change is associated with changes of the entire spectrum. The possibility of measuring spectral response of energy analyzers is discussed in conjunction with the comparison of spectra taken with different analyzers.

Keywords: Secondary electron image brightness, contrast, total yield, channelling effect, electron spectra, work function change, electron beam damage, spectral response.

INTRODUCTION

The scanning electron miscroscope (SEM) is a very useful tool for surface examination. Contrast in a secondary electron image (SEI) arises whenever there are differences in one or more of the following properties: surface topography, crystallographic orientation, chemical composition, surface electric field, specimen conductivity, surface magnetic field and surface potential (Booker, 1969; Thornton, 1968). These widely varied sources of contrast enable us to use SEI to study different surface properties. On the other hand, this complexity also makes the interpretation of SEI difficult. Attempts to correlate image contrast with surface properties (except, perhaps, the topography of non-crystalline samples) are frequently ambiguous or incorrect. The problems often come from poor vacuum conditions, lack of SEI detector calibration, and, more importantly, absence of relating studies of electron spectroscopy in a conventional SEI. The electronic adjustments of image brightness and contrast and of detector spectral response only further obscure the physical meaning of SEI contrast (Appendix I).

Basic studies of electron-solid interaction and secondary emission mechanism should help us unravel SEI contrasts. The combination of SEM with an electron spectrometer in an ultra high vacuum chamber provides *in situ* correlation between SEI and electron spectra. It facilitates, in addition to conventional SEI, other image modes: Auger electron image (AEI), absorbed current image (ACI), energy loss image (ELI) and other images formed by electrons of selected energies. The contrasts of these images are subject to the same influence from various surface properties as that of conventional SEI. This combined instrument will greatly improve our understanding of SEI contrast and make SEM an even more powerful tool for surface science.

In this paper, we summarize our up-to-date work (Lee-Deacon et al., 1982; Le Gressus et al., 1982; Duraud et al., 1980; Geller et al., 1981; Ichinokawa et al., 1981; Le Gressus et al., 1981; Le Gressus et al., 1979; Fontaine et al., 1982) in the development of analytical application (as opposed to pure topographical application) of SEM. We first show the quantitative correlation among SEI brightness, total electron yield, and the integration of electron energy distribution. The results will be used to discuss the origin of crystallographic effect on SEI contrast. We then discuss the relative contribu-

tion of SEI brightness from electrons of different energy domains and the role of work function change in SEI brightness change during gas exposure. Both topics are discussed in conjunction with electron spectra. Electron beam damage on oxygen exposed aluminium surfaces is used as an example to demonstrate the application of electron spectroscopy in SEI interpretation. Finally, we compare spectra taken with a cylindrical mirror analyzer (CMA) and a hemispherical analyzer (HMA) and discuss the possibility of judging the spectral response of an energy analyzer.

Other surface study tools, such as secondary ion mass spectroscopy (SIMS), low energy electron diffraction (LEED) and reflection high energy electron diffraction (RHEED), can also be combined with SEM and provide additional information of surface. In appendix II, we give an example of the correlation between absorbed current image (ACI) and RHEED patterns taken on a Si(111) surface with evaporated Au film. The application of this combination is also discussed.

EXPERIMENTS

Experiments were carried out on an aluminium polycrystal sample in two different machines. The sample surface consisted of large grains (1 $\sim$ 2 mm) and was textured within a few degrees of [111] direction. It was mechanically polished, ion etched and then annealed in the vacuum chamber until no trace of carbon and oxygen was observed with Auger spectrum. The surface plasmon loss peak was sharply defined with primary electron energy (Ep) at 250 eV.

One of the machines used is a JAMP-10(JEOL) with a hemi-CMA whose axis is on the plane of the sample surface. The primary beam has normal incidence. The axis of the SEI detector (Appendix I) is also on the plane of the sample surface and is 90° to the CMA axis. The other machine is an ESCALAB-Mark-II (V.G. Scientific) which is equipped with an HMA (Le Gressus et al., 1982).

The electron spectrum can be obtained either in the integration mode (En(E)) or in the first and second derivative modes (E dn/dE and E d^2n/dE^2) in JAMP-10, while all these spectra plus the electron energy distribution (EED), n(E), can be obtained in the Mark II. With JAMP-10, n(E) can be derived from the En(E) spectrum by multiplying the spectrum by Ep/E. The integration of EED (Duraud et al., 1980) was obtained with a computer,

$$S = \int_0^{Ep} n(E)dE.$$

The quantitative measure of SEI brightness (B) is the output of the SEI detector which was measured with a digital voltmeter. Primary current (Ip) was measured with a Faraday cup on the sample holder. Total sample emission current (Is) was obtained by subtracting absorbed current (Ia) from Ip, i.e., Is = Ip − Ia. Total electron yield (σ) is Is/Ip.

All measurements were obtained with a defocused primary beam in order to avoid beam damage (see further discussion) and to average out the effects of microstructure on the surfaces (topographic features in the order of 1 μm).

LIST OF SYMBOLS

ACI	= Absorbed Current Image
AEI	= Auger Electron Image
ELI	= Energy Loss Image
SEI	= Secondary Electron Image
SEM	= Scanning Electron Microscope
CMA	= Cylindrical Mirror Analyzer
HMA	= Hemispherical Analyzer
Ep	= Primary Energy
B	= Brightness of SEI; SEI detector output
Ip	= Primary Current
Ia	= Absorbed Current
Is	= Total Emission Current; Is = Ip − Ia
σ	= Total Electron yield; σ = Is/Ip
EED	= Electron Energy Distribution; n(E)
S	= Integration of EED; $S = \int_0^{Ep} n(E)dE$
n(E)	= Number of electrons of energy E
δ	= Electron yield
SIMS	= Secondary Ion Mass Spectrometer
LEED	= Low Energy Electron Diffraction
CAE	= Constant Analyzer Energy
SE	= Secondary Emission
UHV	= Ultra High Vacuum
SP	= Surface Plasmon
E	= Energy

RESULTS AND DISCUSSION

1. SEI Detector Calibration

As the first step toward quantitative application of SEM, we set out to investigate the spectral response and acceptance angle of the SEI detector (Lee-Deacon et al., 1982). We measured the relationship between B and Is on eight different grains on the sample surface and with seven different primary energies.

The experiment was carried out in JAMP-10. No collector bias was applied to the SEI detector. The SEI brightness and contrast control (i.e. the controls of the power supply for the photomultiplier) were so adjusted that the SEI output was near zero when the primary beam was turned off. This near-zero value was subtracted from all the SEI detector output to obtain values of B. These settings were kept the same throughout the experiment.

The value of B was found to be a linear function of Is, independent of Ep and grain orientation. (Fig. 1(a) shows B vs. Is of eight grains at six primary energies: 5 keV, 3 keV, 2 keV, 1 keV, 750 eV and 500 eV. Ip was kept at 1×10^{-10}A in all cases. Fig. 1(b) shows B vs. Is of three grains at 5 keV and 250 eV with Ip varying between 3×10^{-10}A and 3×10^{-11}A.

The linearity of B − Is relationship was expected; however, its independence from Ep and crystal orientation was unexpected. Because primary electrons with different energies induce different emission spectra (including the elastically scattered primary electrons), our results indicate that the SEI detector has a broad spectral response. This is different

from what is generally accepted (Booker, 1969; Thornton, 1968), that the SEI detector is more efficient in collecting low energy secondary electrons than collecting high energy primary electrons. Our results also indicate that the SEI has a wide acceptance angle. This point will be discussed later.

2. Correlation between Is and the Integration of EED

The second step approaching an analytical SEM is to correlate the SEI detector with the energy analyzer using emission current as the medium.

We measured (Le Gressus et al., 1982) the change of σ of aluminium under oxygen exposure and compared it with the change of S. This experiment was performed in both JAMP-10 and Mark-II. The results are presented in Table 1. A good correspondence between $\Delta\sigma/\sigma$ and $\Delta S/S$ was obtained on both machines. A similar result has been observed with Si in JAMP-10 (Geller et al., 1981).

The linear relationships between B and Is and between σ and S imply that B is linearly related to S. Changes in EED will be reflected in changes in SEI contrast and brightness, with the rare exception, when the changes in EED do not affect its integration.

3. Electron Channelling Effect vs. Diffraction

An excellent demonstration of the correspondence between electron yield and SEI brightness is given in Fig. 2. Values of σ from three adjacent grains with Ep between 100 eV and 750 eV are shown. Electron yields from these three grains are different and the contrasts of SEI reflect the relative values of σ. The crossover of σ(Ep) curves of grain 1 and grain 2 at around 570 eV corresponds to the contrast reversal between these two grains in the images taken at 500 eV and 750 eV (Fig. 2). The contrast between these two grains is subtle, but definitely detectable, and reflects the small difference in electron yields between these two grains. Grain 3, which is very dark in both images, has low electron yield at all energies.

SEI contrasts among crystal grains on a chemically uniform and flat surface (such as the sample we used) are often ascribed as due to diffraction of the incident electron beam. However, the independence of the linear relationship of B and Is from crystal orientation and from primary energy leads us to conclude that the SEI detector has a wide acceptance angle. It is unlikely that the SEI detector can "see" the space distribution of emitted electrons. SEI brightness depends only on the total electron yield and diffraction effect is not the cause of contrast among grains. Rather, the channelling effect, which describes the crystallographic dependence of electron yield, is more likely to be the reason. We have observed (Ichinokawa et al., 1981) the variation of relative intensities between surface and bulk plasmon losses among different grains on an aluminium surface. The variation was seen both in energy loss spectra and in energy loss images. The sensitive dependence of the channelling direction on the incidence angle of the primary beam is demonstrated in Fig. 3. Pronounced change in SEI contrast among grains was seen when the sample was tilted only 5°.

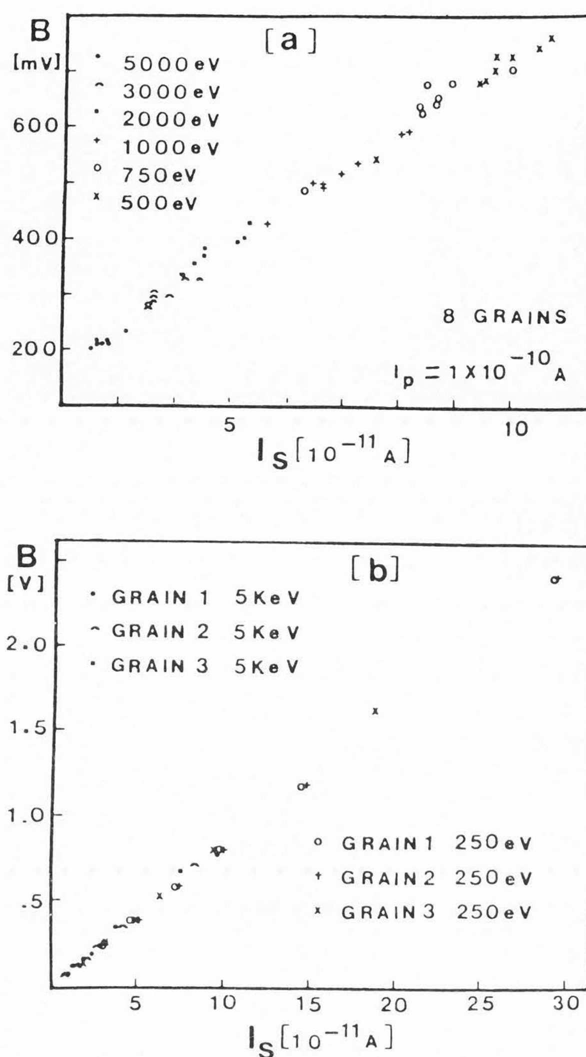

Fig. 1 **Secondary electron image brightness (B) vs. total emission current (Is), (a) of eight grains at six primary energies with constant primary current, 1×10^{-10} A and (b) of three grains at 5 keV and 250 eV with primary current ranging between 3×10^{-10}A and 3×10^{-11}A.**

Table 1. Changes of total yield (σ) and the integration of EED (S) of aluminium (111) surface due to oxygen exposure measured with CMA and HMA.

Analyzer	CMA (JAMP-10)		HMA (Mark-II)	
Ep	250 eV		200 eV	
O_2	OL	1000L	OL	1000L
σ	0.89	1.03	0.93	1.13
$\Delta\sigma/\sigma$	–	15%	–	20%
$\Delta S/S$	–	17%	–	20%

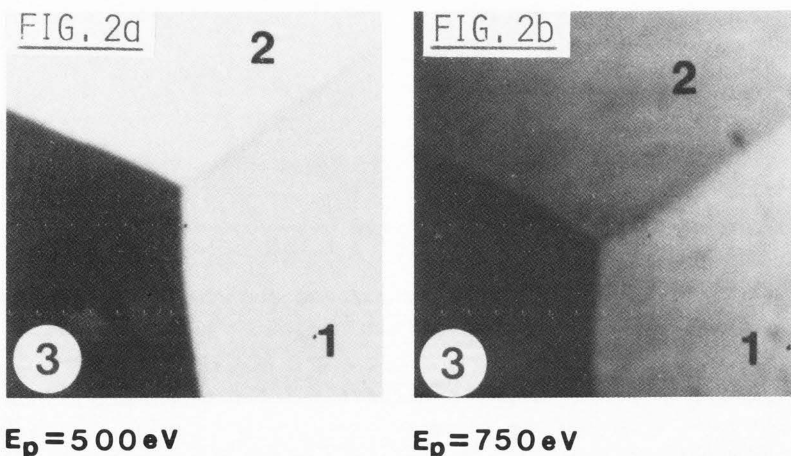

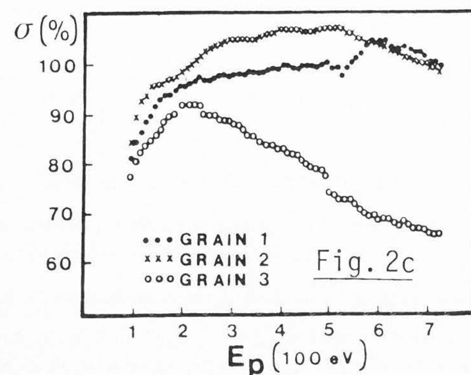

Fig. 2. Total electron yield (σ) vs. primary energy (Ep) of three different grains and two secondary electron images taken at 500 eV and 750 eV. The reverse of contrast between grains 1 and 2 in these two images corresponds to the crossover of the σ(Ep) curves.

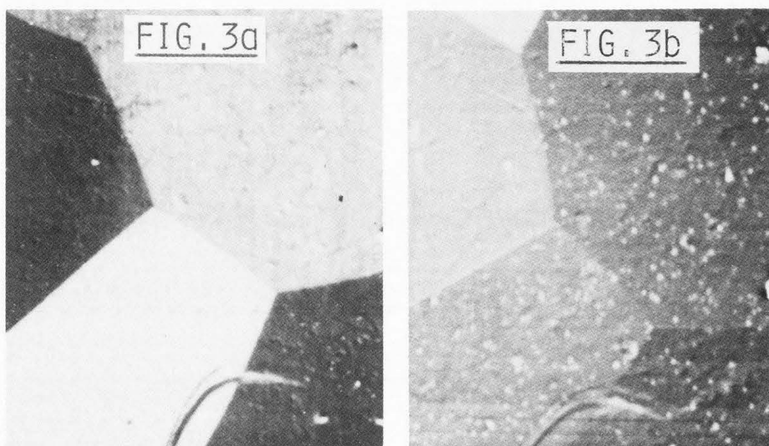

Fig. 3. SEI of an aluminium polycrystal surface taken at two different primary beam incidence angles, (a) 0° (b) ∿ 5°. Both images were taken with Ep = 230 eV.

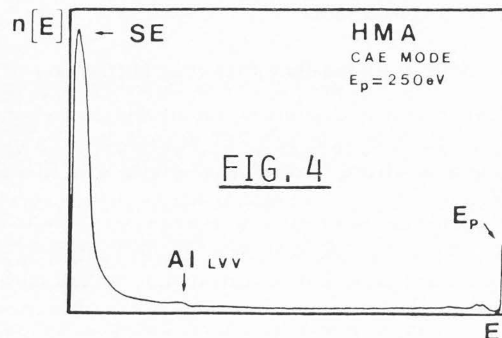

Fig. 4. Electron energy distribution, n(E) of clean aluminium surface obtained with a hemispherical analyzer, operating at constant analyzer energy (CAE) mode. Ep = 250 eV.

4. Contribution of Secondary Electrons to SEI Brightness

Fig. 4 is the n(E) spectrum of a clean Al surface obtained with Mark-II operating at constant analyzer energy (CAE) mode with EP = 250 eV. The spectrum reveals that the true secondary emission (SE) contributes to about ⅔ of the total emission. Therefore, SEI brightness is largely due to true secondary electrons.

Although this conclusion is the same as generally accepted (Booker, 1969; Thornton, 1968), the reasoning is quite different. As pointed out previously, we think that our experiments show a broad spectral response of SEI detector. The high contribution of true secondary electrons to SEI brightness is based on spectral structure. Other authors (Booker, 1969; Thornton, 1968) however based their case on the different effective acceptance angles for electrons of different energies. A study to calculate the trajectory of electrons, considering the electrical field distribution caused by the voltages applied to SEI detector (Appendix I), will help to clarify this point.

5. The Role of Work Function

The major cause of SEI brightness change during gas contamination is said to be the change of work functions (Holm and Reifandt, 1978). To verify this point, we compared the electron spectra of aluminium surface before and after oxygen exposure. The experiment was performed in Mark-II with Ep at 200 eV and in JAMP-10 with Ep = 250 eV. The spectra taken in Mark-II are shown in Fig. 5. The difference between the spectra of a clean surface and of a 1000 L exposed surface was calculated by a computer and is shown in the bottom half of Fig. 5. The decrease of surface plasmon (SP) and the change of the energy loss spectrum were accompanied by the decrease of secondary electron emission. The contribution of the plasmon decay to the secondary electron emission remained weak (Ganachaud and Cailler, 1979). However, the largest change in the spectrum occurred at energies around 20 eV and higher. Table 2 shows the contribution to the change of S from different energy domains. A similar experiment has been carried out on an Si surface with CMA (Geller et al., 1981). It showed that after 10^4 L oxygen exposure, the entire spectrum increased, except the plasmon loss region which decreased.

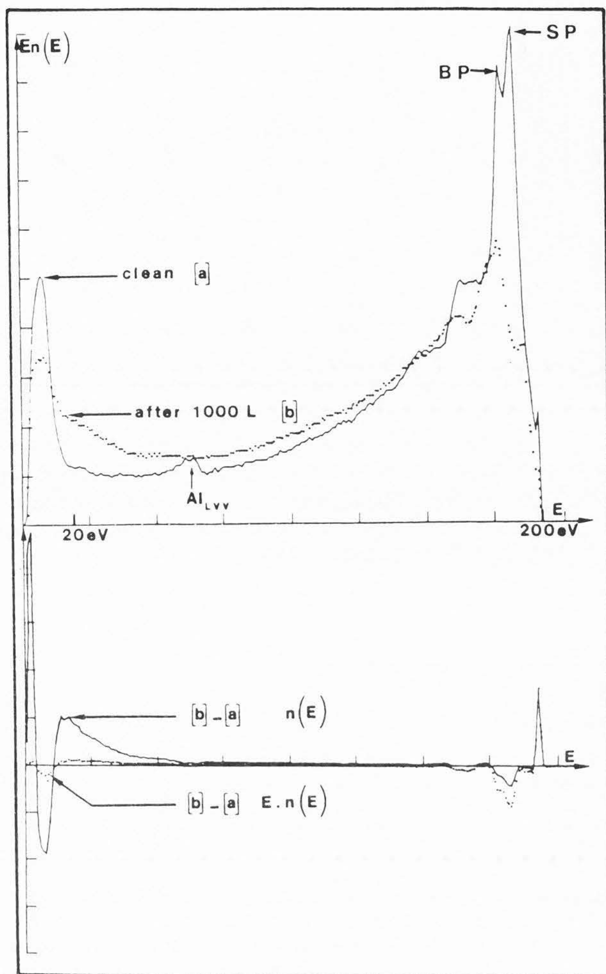

Fig. 5. Electron spectra, En(E) of aluminium surface (a) when it was clean and (b) after it had been exposed to 1000 L oxygen. The difference between (a) and (b) was obtained with a computer and is shown in the bottom half of the figure.

Table 2. Contribution of changes in the integration of EED (S) from different energy ranges during oxygen exposure on aluminium surface.

$$S_i = \int_{E_{1i}}^{E_{2i}} n(E)dE \; ; \; \Delta S_i = (S_i)_{1000L} - (S_i)_{0L}$$

	E_{1i}	E_{2i}	Results CMA	HMA
$\Delta S/S$	0	Ep	17%	20%
$\Delta S_1/S$	0	8 eV	−0.5%	0.3%
$\Delta S_2/S$	0	30 eV	0.6%	10%
$\Delta S_3/S$	30 eV	Ep − 30eV	13.4%	9%
$\Delta S_4/S$	Ep − 30eV	Ep	3%	0.3%

The appearance of the emission around 20 eV after oxygen exposure can be explained as either due to the decay of volume plasmon of alumina (Benndorf et al., 1977) or due to the scattering of backscattered electrons by oxygen 2S electrons. We are more in favor of the latter explanation because the spectrum changed over the entire energy region. This change corresponds to the modification of elastic mean free path when the surface is oxidized.

Our results clearly point out that work function change alone cannot explain the changes of electron spectrum and total electron yield, and thus it cannot be the major cause of SEI brightness change during oxygen exposure. Rather, the change in the energy loss process related to oxidation is a better explanation.

6. Electron Radiation Effect and SEI Brightness Change

The importance and usefulness of the collaboration of SEM and electron spectrometer are illustrated by the role of spectrometer in clarifying the cause of SEI brightness change during electron irradiation in ultra high vacuum. SEI darkening in SEM was usually understood as due to carbon deposition under the primary beam (Holm, Reifandt, 1978; Soezima, 1979). However, this explanation is improper for the effect observed in an ultra high vacuum system.

We studied the SEI brightness change on oxygen-exposed aluminium surfaces with the aid of Auger electron spectroscopy (Le Gressus et al., 1981; Fontaine et al., 1982). Fig. 6 shows the Auger electron spectra of an oxygen exposed (1000 L) aluminium (111) surface at several stages during electron irradiation. The 68 eV peak is the Al LVV peak and the 56 eV peak is the interatomic Auger transition of oxidized aluminium. Spectrum 1 was taken right after oxygen exposure. It is observed that the 68 eV peak increased while the 56 eV peak decreased as the surface was irradiated with 230 eV electrons (spectra 1 to 3). This indicated a decrease of oxidation within the irradiated area. In SEI, this area became darker than the surroundings (image 3, Figure 6). This phenomenon corresponds well to the lower electron yield at lower oxygen exposure (refer to e.g. Table 1). When the electron energy was changed to 5 keV, the relative intensity of these two peaks reversed (spectra 4 and 5) and the irradiated area became brighter than the non-irradiated area (note that image 5 was taken with Ep = 230 eV). Again, the brightening can be correlated with the increase of oxidation and thus the increase of electron yield within the area. After the 5 keV irradiation, the ratio between the two peaks was stable when the area was again irradiated with 230 eV electrons (in spectra 6 to 8).

The SEI brightness change on an oxygen exposed aluminium surface during electron irradiation is clearly linked to the change of oxidation and is not due to carbon contamination. Work function change alone cannot also explain this effect. A detailed study of this phenomenon will be published elsewhere (Fontaine et al., 1982). Based on the study of Auger electron spectroscopy, we were able to explain the change of oxidation extent and thus the change of SEI brightness as due to electron beam assisted surface diffusion of chemisorbed oxygen and transformation of chemisorbed oxygen into oxide.

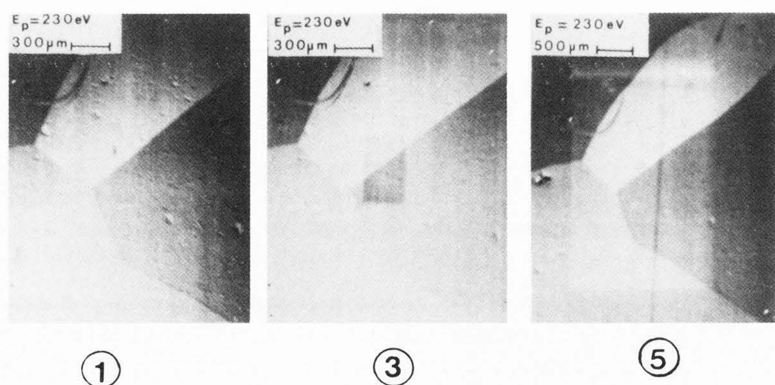

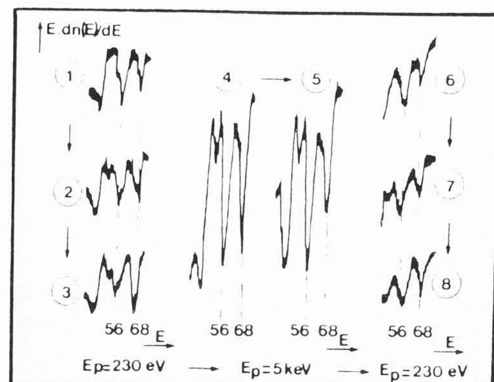

Fig. 6. **Auger electron spectra of aluminium surface with 1000 L oxygen exposure during different stages of electron irradiation: spectra 1 to 3 were taken at Ep = 230 eV. Spectra 4 and 5 were Ep = 5 keV. Spectra 6 to 8 were taken with Ep = 230 eV again. All spectra were taken with Ip = 5 × 10^{-9}A. The spectra are numbered according to the order of their acquisition. Acquisition time for each spectrum was 80 seconds. The secondary images correspond to the irradiation stages as identified by the numbers. All images were taken with Ep = 230 eV.**

7. Comparison between HMA and CMA – an ultimate electron energy analyzer?

For use as a quantitative analytical tool, an electron energy analyzer has to detect electron energy distribution without distortion, or at least, to have known spectral response. Absolute intensity (i.e. peak height) and energy calibration of an energy analyzer can be achieved through comparison between experimental and theoretical results of electron spectra. Unfortunately, complete theoretical descriptions of secondary emission and of electron-solid interactions are not available. As a preliminary test, we studied the reproducibility of spectra with different energy analyzers. This kind of comparison will help us to define the problems in energy analyzer calibration.

We performed such a study comparing spectra obtained from a CMA (JAMP-10) and an HMA (Mark-II) on aluminium surfaces. Full account of this study will be published in another report (Le Gressus et al., 1982); we will only present a brief summary here.

Fig. 7 shows the dn/dE spectra in the secondary emission region of a clean aluminium surface taken with CMA and with HMA. These two spectra are very similar. The peaks at 5.2 eV and 11 eV and the shoulder of 7 eV in the CMA spectrum showed up in the HMA spectrum at 9 eV, 15 eV and 11 eV, respectively. The difference in energy position is due to different energy references used in these two spectrometers — Fermi level in HMA and Fermi level minus analyzer work function in CMA. The peak at around 15 eV and the shoulder at around 11 eV (refer to HMA spectrum) are due to plasmon decay (Ganachaud, Cailler, 1979). The first SE peak, at 9 eV, corresponds to the maximum slope in En(E) spectrum. It has been observed (Le Gressus et al., 1982) that it shifted about 1 $\sim$ 2 eV when the surface was slightly contaminated and the surface plasmon loss peak was damped. This shift of energy has been explained (Le Gressus et al., 1981) as due to sample work function change and agrees with results obtained with a Kelvin probe (Hofmann et al., 1979).

When we compare the En(E) spectra taken with these two analyzers (Fig. 8), we observe that the plasmon loss peaks are

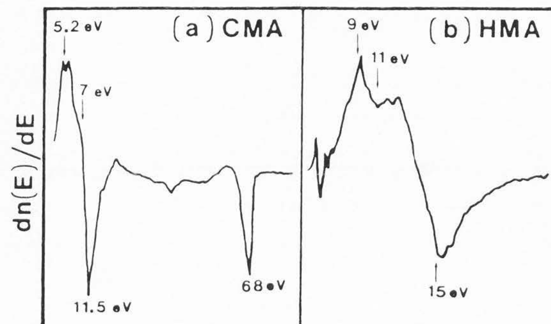

Fig. 7. **dn(E)/dE spectra of a clean aluminium surface taken with CMA (JAMP-10) and HMA (Mark-II).**

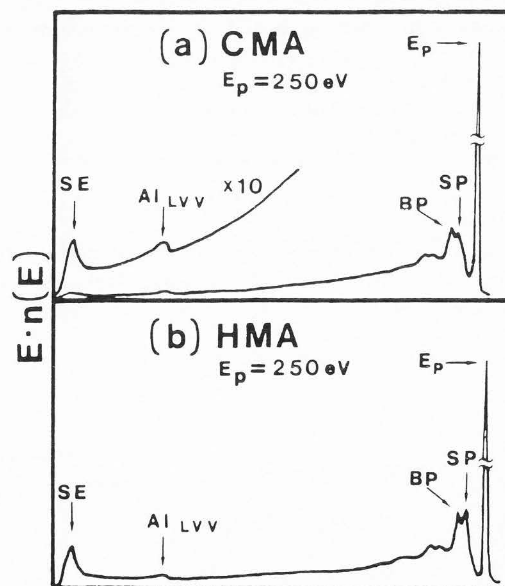

Fig. 8. **En(E) spectra of a clean aluminium surface taken with CMA (JAMP-10) and HMA (Mark-II). The secondary emission (SE) and Al LVV peak have different relative intensities in these two spectra.**

very intense in both spectra. However, the relative intensities of SE and Auger peaks are different in these two cases. This difference is likely to stem from different geometry (spatial arrangement among the sample, the incident beam and the detector) and energy response functions of these two analyzers. The latter could be partially due to the electronic circuit design of the electron multiplier in the analyzer.

It is impossible to judge which analyzer gives spectra closer to the "true" ones without more studies and comparison with theoretical results. We suggest that the intensity of the first SE peak and its change due to work function change might serve as a guide to the intensity calibration of the energy analyzer in the low energy range. The general shape of the background of a spectrum is related to electron scattering and is sensitive to atomic number and mean free path change (Le Gressus et al., 1982; Pellerin et al., 1981; Ichimura et al., 1980; Duraud et al., 1980). It perhaps can serve as a reference in the intermediate energy region.

CONCLUSIONS

Our studies of analytical application of SEM combined with electron spectroscopy lead us to the following conclusions:

(1) SEI brightness is proportional to the total electron yield, independent of primary electron energy and crystal orientation.

(2) SEI detector of Everhart and Thornley type has wide acceptance angle and broad spectral response.

(3) Crystallographic effect of SEI contrast is more likely due to electron channelling than electron diffraction.

(4) Secondary electron emission constitutes the major part of SEI signal because it is the main component of total electron yield.

(5) Changes in the entire electron spectrum are responsible for the SEI brightness change during gas exposure; the work function change alone cannot account for the brightness change.

(6) Electrom beam damage effect is the cause of SEI brightness change during image or spectrum acquisition in UHV, carbon deposition is not.

The necessity of applying in situ measurement of electron spectra to correctly interpret electron images is clearly demonstrated in our work. Further theoretical and experimental studies are much desired in order to fully explore the potential of SEM in surface science studies.

APPENDIX I

The SEI detector in JAMP-10 is a scintillator/light pipe/photomultiplier system of Everhart and Thornley (Everhart and Thornley, 1960) as shown in Fig. A-1. The scintillator is at + 10 kv relative to ground. Positive or negative bias can be applied to the collector. All electrons which enter the collector will gain 10 keV before they strike the scintillator. The photon yield of the scintillator is therefore not sensitive to the initial energy of the collected electrons as long as this energy is small compared to 10 keV.

The operation parameters of the SEI detector can affect image contrast. An example is given in Fig. A-2. Fig. A-2(a) shows an SEI of a steel surface with segregated SiO_2. The image was taken without bias voltage on the collector of the SEI detector. When a negative bias was applied to the collector,

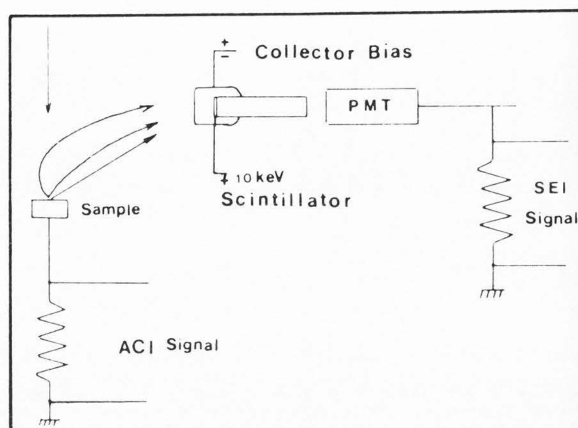

Fig. A-1. Diagram illustrating a SEI detector — a scintillator/light-pipe/photomultiplier system of Everhart and Thornley (Everhart and Thornley, 1960).

with all other things unchanged, the SEI contrast reversed completely, as shown in Fig. A-2(b). This change of contrast is due to different energy distributions of electrons from steel and SiO_2 and low energy electrons are prevented from entering the collector by the applied negative voltage.

Furthermore, the operation parameters of the SEI detector affect not only the number of electrons detected but also the number of electrons emitted from the sample. This effect is demonstrated in Fig. A-3. Absorbed current images (ACI) were taken from a contaminated Si surface on which contrasting areas had been produced by various degrees of electron radiation damages. ACI is the "negative" of the emission current image and is independent of the detection functions (acceptance angle, spectral response, etc.) of the SEI detector. Its contrast represents the variations of electron yield (δ) over the surface. Figs. A-3(a) - A-3(d) show that relative values of electron yield at different areas changed as the voltages applied to SEI detector changed. The changes in electrical field inside the analyzing chamber clearly affected the sample surface potential and caused the changes in electron yields. The ACI contrast changed accordingly.

APPENDIX II

Submonolayer coverage of surface contamination can cause SEI brightness change. Fig. A-4 shows the negative of an absorbed current image (ACI) of a Si(111) surface on which a thin layer of Au has been evaporated.The image brightness is not uniform — bright spots surrounded by intermediate shaded areas on a dark background. Reflective high energy electron diffraction patterns (RHEED) show that the contrasts are due to different coverages of Au on the surface. Low energy electron diffraction (LEED) is expected to have the same capability of distinguishing coverage differences.

This example shows the aid of electron diffraction (RHEED and LEED) in identifying electron image features. On the other hand, one can use the high resolution of SEM to improve the resolution of the electron diffraction (RHEED of LEED) technique. For example, one can calibrate the electron image brightness against coverage of a particular thin film-substrate system by means of electron diffraction. A high resolution SEM image (SEI, AEI or ACI, etc.) can then be used to identify the spatial variation of thin layer coverage with a resolution which is not normally attainable with diffraction technique.

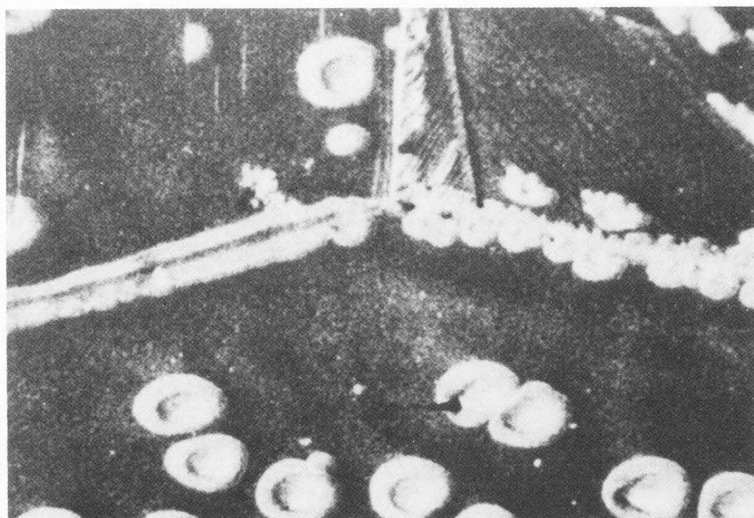

[a] zero bias

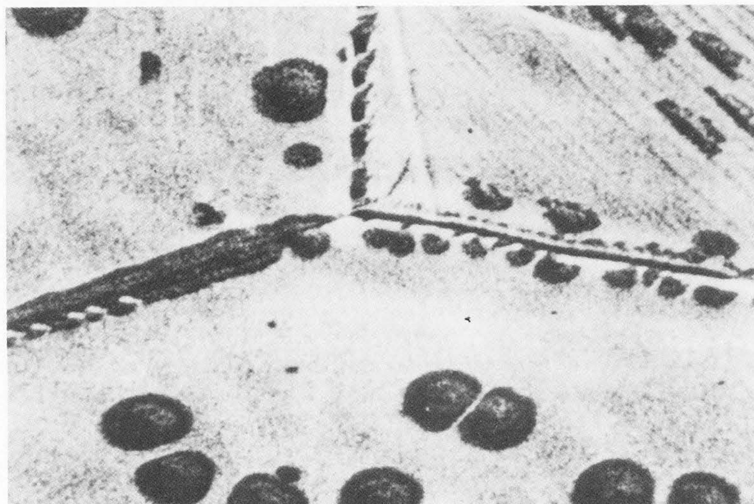

[b] negative bias

Fig. A-2. SEI of a steel surface with segregated SiO_2, (a) without collector bias, (b) collector bias − 200 V.

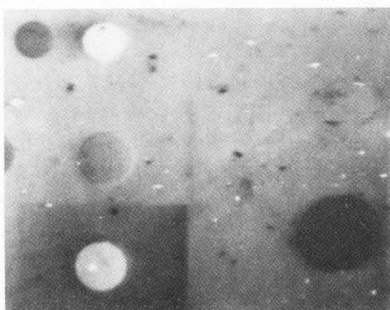

[a] ACI C: 0V S: OFF

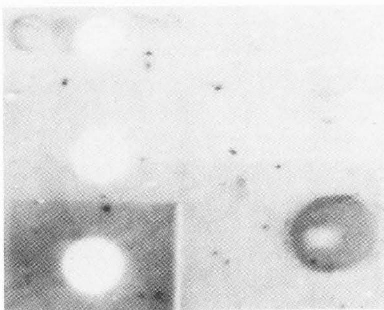

[b] ACI C: 0V S: 10KV

C: COLLECTOR BIAS S: SCINTILLATOR

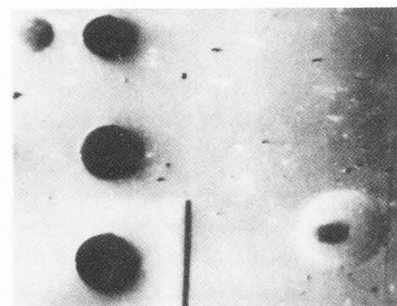

[f] SEI C: 0V S: 10KV

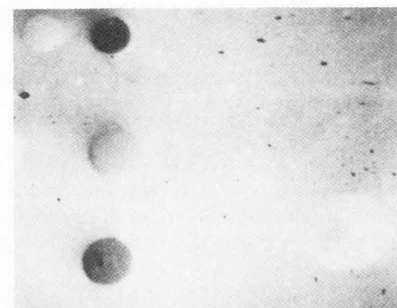

[e] SEI C: +200V S: 10KV

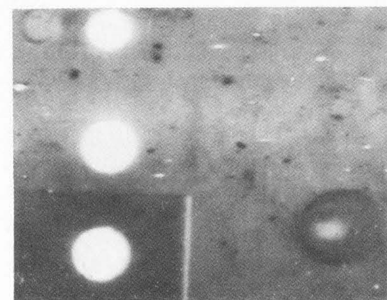

[d] ACI C: +200V S: 10KV

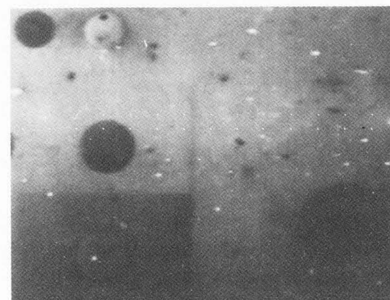

[c] ACI C: −200V S: 10KV

Fig. A-3.
ACI and SEI of a contaminated Si surface with various collector bias voltages and scintillator high voltage. Patches of different contrasts were produced by different degrees of electron radiation damage.

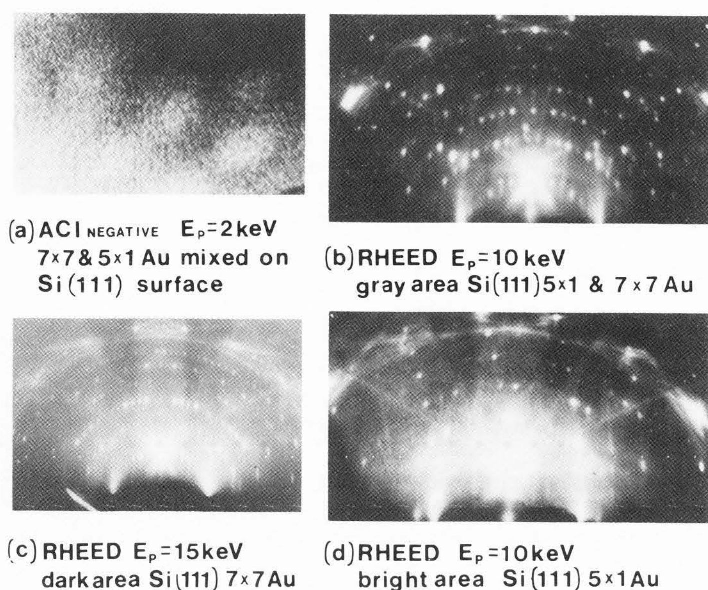

Fig. A-4.

(a) The negative of an ACI of a Si(III) surface with evaporated Au film. Contrast is due to different coverage of Au.

(b) - (d) RHEED patterns taken from different areas of the sample showing sub-monolayer coverages of Au on (7 × 7) silicon. (Photos courtesy of T. Ichinokawa).

REFERENCES

Benndorf C, Keller G, Seider H. (1977). ELS investigations of the beginning oxidation on aluminium thin film. Surf. Sci. **67**, 589-595.

Booker GR. (1969). Modern diffraction and imaging techniques in materials science, in: Proceedings of the International Summer Course on Material Science, Antwerp, Belgium, July 28-August 8, 1969, S. Amelinckx, R. Gevers, G. Remut and J. Van Landuyt, (eds.), North Holland, Amsterdam, 553-595.

Duraud JP, Le Gressus C, Massignon D, Ichimura S. (1980). Atomic number background dependence in Auger electron spectroscopy, in: Proceedings 4th International Conf. on Solid Surf. and 3rd European Conf. on Surf. Sci., September 22-26, 1980, Cannes, France, J.D. Degras, C. Costa (eds.), French Vaccum Society, Paris Publishers, 922-925.

Duraud JP, Le Gressus C, Massignon D, Pellerin F. (1980). Image contrasts in ultra-high vacuum SEM, Scanning Electron Microsc. 1980: **IV**: 49-54.

Everhart TE, Thornley FM. (1960). Wide-band detector for micro-microampere low energy electron currents. J. Sci. Inst. **37**, 246-248.

Fontaine JM, Lee-Deacon O, Duraud JP, Ichimura S, Le Gressus C. (1982). Electron beam effects on oxygen exposed aluminium surfaces. Surf. Sci. **122**, 40-54.

Ganachaud JP, Cailler M. (1979). A Monte-Carlo calculation of the secondary electron emission of normal metals. II. Results for Aluminium. Surf. Sci. **83**, 519-530.

Geller J, Pellerin F, Le Gressus C. (1981). Electron spectroscopy of silicon as modified by oxygen exposure, Scanning Electron Microsc. 1981; **IV**: 295-300.

Hofmann P, Wyrobisch W, Bradshaw AM. (1979). The interaction of oxygen with alumnium single crystal: Mainly $\Delta\phi$ aspects. Surf. Sci. **80**, 344-351.

Holm R, Reifandt B. (1978). Auger analysis in a conventional scanning electron microscope. Scanning **1**, 42-57.

Ichimura S, Le Gressus C, Shimizu R. (1980). Etude du fond continu associé à l'emission d'électrons Auger. C.R. Acad. Sci. Paris, **291**, B67-B70.

Ichinokawa T, Le Gressus C, Mogami A, Pellerin F, Massignon D. (1981). Variation of relative intensities between surface and bulk plasmon losses due to crystal orientation for aluminium in low energy electron reflection loss spectroscopy. Surf. Sci. **111**, L675-L679.

Lee-Deacon O, Le Gressus C, Duraud JP, Massignon D. (1983). Channelling effect on SEI contrast, Scanning Electron Microsc. 1983; II:537-542.

Le Gressus C, Lee-Deacon O, Yates K, West R. (1983). Reproducibility of electron spectroscopy data with CMA and HMA: AES, ELS and SES on clean aluminium, Scanning Electron Microsc. 1983; I:77-84.

Le Gressus C, Massignon D, Mogami A, Okuzumi H. (1979). Secondary electron emission dependence on electron beam density dose and surface interactions from AES and ELS in an ultra-high vacuum SEM, Scanning Electron Microsc. 1979; **I**: 161-172.

Le Gressus C, Okuzumi H, Massignon D. (1981). Changes of SEI brightness under electron irradiation as studied by electron spectroscopy, Scanning Electron Microsc. 1981; **I**: 251-261.

Pellerin F, Le Gressus C, Massignon D. (1981). A secondary electron spectroscopy and electron energy loss spectroscopy study of the interaction of oxygen with a polycrystalline aluminium surface. Surf. Sci. **103**, 510-523.

Soezima H. (1979). Solid surface observation at very low accelerating voltage (200 V-1 kV) by Scanning Electron Microscopy, Surf. Sci. **86**, 610-619.

Thornton PR. (1968). Scanning Electron Microscopy, Chapman and Hall, London, 13-25, 188-215.